Nuclear Inst. and Methods in Physics Research, A 1055 (2023) 168531

Contents lists available at ScienceDirect

Nuclear Inst. and Methods in Physics Research, A

journal homepage: www.elsevier.com/locate/nima

Full Length Article

Extracting clean low-energy spectra from silicon strip detector telescopes around punch through energies

E.A.M. Jensen *, K. Riisager, H.O.U. Fynbo

Institut for Fysik & Astronomi, Aarhus Universitet, DK-8000, Aarhus C, Denmark

ARTICLE INFO

Keywords:
Silicon strip detector
Detector telescope
Punch through
Energy loss
Stopping
^{21}Mg

ABSTRACT

The response of detector telescopes becomes complex around their relevant punch through energies: For some deposited energies the corresponding particle kinetic energies cannot be uniquely assigned, and these spurious energy regions can span several hundreds of keV if the telescopes are employed in close geometry. We present methods for producing clean low-energy spectra of light ions from detector telescopes consisting of thin double-sided silicon strip detectors (DSSSDs) backed by thick silicon pad detectors. By following these methods, the spectra of several such detector telescopes can be combined to span the entire relevant particle energy spectrum, above as well as below the punch through thresholds of the individual telescopes. The total energy spectrum resulting from the combination of all telescope spectra thus encompass the entire particle energy distribution in conjunction with the energy-dependent, setup-specific solid angle coverage. Energy spectra of beta-delayed proton emission from ^{21}Mg are used to illustrate the methods.

1. Introduction

The utilisation of detector telescopes to distinguish types of atomic nuclei and determine their initial kinetic energies in nuclear reaction and decay experiments with the so-called ΔE-E *technique* is well-established [1,2], and the technique is continuously being refined and adapted for specialised detection designs at low, intermediate and high energies — see e.g. Ref. [3] for a recent review. The correlated energy depositions in a thin ΔE detector and the thicker E detector are characteristic of the type of particle which first deposits a fraction of its initial energy in the ΔE detector, then *punches through* to the E detector and, finally, deposits the remainder of its energy in the E detector. Depending on the needs of the experiment, the correlated signals for various telescope events can be compared e.g. by the *power law scheme* described in [1], or the energy depositions can be compared to energy loss tabulations provided e.g. by *SRIM* [4] or *ICRU* [5,6], thus providing a particle identification (PID) method.

While the PID provided by utilising detector telescopes is an invaluable feature, in this paper the focus is on how energy spectra of detector telescopes can be properly extended below the *punch through thresholds* of the individual ΔE detectors. By extending the energy spectra below the punch through thresholds, the dynamic ranges of the detector telescopes becomes not only that of the combined $\Delta E - E$ configuration but also that of the ΔE detector on its own. Employing the entire dynamic range of a given detector telescope in this way can be very attractive for some nuclear physics cases. There are, however, inherent problems involved in extending the energy spectra below the punch through thresholds, and, depending on the data at hand, the problems might not be immediately obvious from the resulting combined spectra alone. In this paper, the problems inherent in extending the energy spectra below the punch through thresholds of detector telescopes will be described and their proper handling demonstrated.

The small thicknesses of the ΔE detectors employed in detector telescopes has the advantage of suppressing the beta response of the telescope as a whole. PID cannot be carried out with a given ΔE detector, by itself, below its punch through thresholds (which will vary for different types of particles). This means that prior knowledge or other PID methods must be employed to interpret the particle energy spectra below the relevant punch through thresholds. If the particle spectra, in this sense, can be meaningfully extended below the relevant punch through thresholds, care must still be taken to eliminate various types of distortions at intermediate energies. The distortions primarily appear due to the signal thresholds of the employed E detectors, and the effect will be enhanced if the geometry of the detection setup is close — an otherwise desirable feature. The distortions can potentially span many hundreds of keV of the full energy spectrum at hand.

In experiments where beta-delayed particle emission is studied, properly extending the energy range below the punch through threshold can in principle reveal the entire particle energy spectra — from the characteristically low-lying single-nucleon separation energies of the *emitter* up to the large Q-value of β-decay from the *precursor*; see e.g. Refs. [7,8]. Recent data [9] on beta-delayed proton emission from

* Corresponding author.
E-mail address: ej@phys.au.dk (E.A.M. Jensen).

https://doi.org/10.1016/j.nima.2023.168531
Received 3 June 2023; Accepted 6 July 2023
Available online 9 July 2023

^{21}Mg [10] is used to illustrate the methods which will be developed in this paper. The physics case of ^{21}Mg is quite ideal for these illustration purposes, due both to the beta-delayed proton branch dominating the decay scheme and due to the wide distribution of energy levels across the entire dynamic range of the utilised silicon detector telescopes. While the methods developed here are framed around nuclear decay experiments, the methods should easily extend to low-energy nuclear reaction experiments as well.

The utilised ΔE detectors are double-sided silicon strip detectors (DSSSDs) with 16 × 16 strips spanning an area of 50 × 50 mm^2 with ultra-thin entrance windows [11]. The active layer thicknesses of these detectors are in the range 30–70 μm. The ΔE detectors are situated roughly 40 mm from (and facing) the point of particle emission and are backed by 50 × 50 mm^2 single-sided silicon pad detectors of thicknesses around 500 μm. These E detectors are situated 5 mm behind their corresponding ΔE detectors. A complete description of the experimental setup is given in Ref. [12]. The segmentation of the ΔE detectors provides accurate information of a given particle's trajectory and, in turn, allows for accurate determination of the initial particle energies through energy loss corrections of the particles in the effective dead layers of both ΔE and E detectors. The energy calibrations of the detectors take various dead layer energy losses into account. The response functions of the utilised silicon detectors, while not taken into account here, are well understood [13].

In the following, we start by presenting an overview of the passage of particles through detector telescopes. From this overview it will become clear that care must be taken in extending the energy spectra below the punch through thresholds of ΔE detectors. We will then demonstrate how this can be done with the aid of energy loss tabulations, developing a repertoire of methods. The end result of utilising these methods is the ability to produce full-range particle energy spectra accompanied by energy-dependent, setup-specific solid angle coverages. Data from an experiment studying beta-delayed proton emission from ^{21}Mg will exemplify the development of the methods.

2. Particle passage of detector telescopes

2.1. Stopping

In the following, the stopping of charged particles shall principally concern what is commonly referred to as the *stopping of ions* [4], i.e. the stopping of atomic nuclei — the "ions" may or may not be electrically neutral due to the ionisation of the atoms in question.

As a charged particle impinges on the surface of a slab of material of thickness L_0 at an angle of incidence θ, the length of material traversable by the particle (if the particle energy is sufficiently large) is the effective length of material

$$L_{\text{eff}} = \frac{L_0}{\cos\theta} = L_0 + \Delta L = L_0 + (L_{\text{eff}} - L_0) \tag{1}$$

The effective length L_{eff} is here explicitly split into the minimal length of material L_0 at $\theta = 0$ and the additional component ΔL which contributes at $\theta > 0$. The energy loss E_{loss} experienced by a particle which traverses the entire material is given by

$$E_{\text{loss}} = \int_0^{L_{\text{eff}}} S(E)\mathrm{d}x \simeq S_0 \int_0^{L_{\text{eff}}} \mathrm{d}x = S_0(L_0 + \Delta L) = S_0 L_0 \left(1 + \frac{1-\cos\theta}{\cos\theta}\right) \tag{2}$$

where the stopping power S, which explicitly depends on the particle energy E and implicitly depends on the properties of the particle and the material, is approximated as being a constant S_0 during the particle's entire traversal of the material. While this approximation is generally poor, the functional form of the right-hand side of Eq. (2) will prove useful later on; the expression relates a given energy loss E_{loss} to a given angle of incidence θ for fixed S_0 and L_0. Note that the particle in question is supposed not to veer (measurably) from its initial direction of motion as it traverses the material.

2.2. Electronics

The electronic signals read out from the *active layers* of charged-particle detectors are converted, via energy calibrations, to deposited particle energies. These must be corrected for the energy losses in the detector *dead layers* and any other inactive media the particles might traverse before reaching the active layer of the detector; see e.g. Ref. [14]. Energy loss corrections are made employing energy loss tabulations.

Charged-particle detectors inevitably have some signal threshold under which charged particles cannot meaningfully be separated from electrical noise inherent in the detector. This can be considered an effective (energy-dependent) contribution to the actual physical thickness of the dead layer of the detector. Of course, this effective part of the dead layer does not require energy loss corrections, but it does, effectively, act as a significant obstacle for any particle incident on a given detector.

Here we stress an important point: For modern silicon detectors with low-Z entrance window thicknesses on the sub-micrometer level, the dynamic range towards zero energy (assuming otherwise perfect detector calibrations) for a given silicon detector is primarily constrained by its signal threshold, and *not* by the thickness of its entrance window. Consider, for instance, a proton with an initial kinetic energy of 2.0 MeV which punches through a ΔE silicon detector of 40 μm active layer thickness at normal incidence. The proton deposits roughly 1.4 MeV [4] in the ΔE detector and emerges on the opposite side with 0.6 MeV kinetic energy remaining, bound for impact with a backing E detector. The remaining 0.6 MeV of the proton will be reduced further in the dead layers of the E detector before reaching its active layer — for example by roughly 33 keV in a combined aluminium and silicon dead layer of 0.6 μm. The E detector could, however, conceivably have a signal threshold of 100 keV (at room temperature) which is three times the energy lost in its dead layers. Taking the 33 keV reduction in the dead layer into account, this 100 keV signal threshold corresponds to an additional 1.7 μm dead layer thickness. Based on this example, we state here that the two main parameters of interest for a modern $\Delta E-E$ detector telescope are (1) the signal threshold of the E detector, and (2) the active layer thickness of the ΔE detector. These two parameters characterise, more than anything else, the data extracted from detector telescopes above and below punch through.

The ΔE detectors used as examples in this paper are equipped with 0.1 μm p-doped silicon dead layers (only 3%–4% of the detector surface is covered by electrical contacts) and had signal thresholds around 100 keV. The E detectors are equipped with metallisation on top of p-doped silicon dead layers corresponding to approximately 0.6 μm silicon — their signal thresholds are also roughly 100 keV. Evidently, the example of a proton punching through a ΔE detector of 40 μm active layer thickness and having to overcome the dead layer and signal threshold of the backing E detector is highly relevant. If the angle of incidence between detector surface and the point of particle emission is allowed to vary, a significant portion of the particle energy spectrum will be affected, as we shall now see.

2.3. Types of events

The left part of Fig. 1 schematically depicts the various types of events a charged particle of varying kinetic energy can cause in a charged-particle detector telescope, and the right part of Fig. 1 shows an example of a particle's energy deposition E_{dep} in the active layers of a telescope against its actual kinetic energy E_{p}. The charged particle is emitted – e.g. from a foil with possible spread in source position – towards the detector telescope at some angle of incidence with a given energy. With reference to both the left and right parts of Fig. 1, the following scenarios can occur:

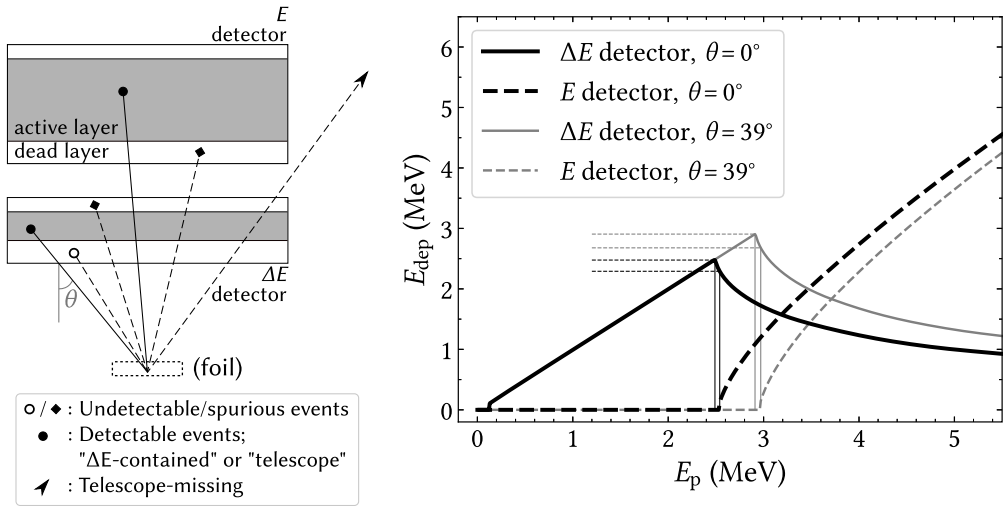

Fig. 1. Left: Illustration of different types of stopping of a charged particle in a detector telescope as it is emitted from a point with various kinetic energies. The layer thicknesses are not meaningfully scaled. **Right:** Example of energy deposition E_{dep} vs. kinetic energy E_{p} of a proton in the active silicon detector layers of a telescope at two extremes of angles of incidence θ. The ΔE detector has a thickness of 67 μm and the E detector has a signal threshold of 100 keV. SRIM [4] has been employed to tabulate the deposited energies. See the text for a discussion of the different types of events.

- Open circle, $E_{\text{p}} \lesssim 0.1$ MeV: The particle is emitted with such low energy that it is stopped in the (effective) dead layer before it reaches the active layer of the ΔE detector. The telescope is blind to this kind of event, which effectively sets the lower limit on the dynamic range of the telescope. We shall denote this type of event an *undetectable event*.
- Closed circle, E_{dep} is increasing with E_{p}: The particle initially has a kinetic energy which allows it to reach one of the two active layers of the telescope before it is completely stopped. These are the ideal types of events. The particle is either stopped in the active layer of the ΔE detector, or it is considerably more energetic and *punches through* the ΔE detector and is then stopped in the active layer of the E detector. Starting from the deposited energy in a given active layer, one can find the original particle energy by employing energy loss tabulations to iteratively calculate the particle's energy prior to its traversal of the effective thicknesses of the preceding layers. Events in which the particle is stopped in the active layer of the ΔE detector we shall denote *ΔE-contained events*, while events in which the particle is stopped in the active layer of the E detector we shall denote *telescope events*.
- Square, E_{dep} is decreasing with E_{p} in the ΔE detector and E_{dep} in the E detector is zero: The particle is sufficiently energetic to *punch through* the active layer of the ΔE detector, but it lacks the necessary energy to *reach through* to the active layer of the E detector. Hence it is stopped in the dead layer of either of the two detectors, between their active layers. As the particle loses more energy in the larger effective layer thicknesses at larger angles of incidence θ (Eq. (2)), the beginning and end of this energy region is inherently dependent on θ. We shall denote the entire θ-dependent region in which the particle is stopped in the dead layers between the two active layers the *dead zone* of the detector telescope. The two black vertical lines in the right part of Fig. 1 exemplifies the boundaries of the dead zone at small θ and the two grey vertical lines at large θ — in this example the entire dead zone, from smallest to largest θ, spans 400 keV. We shall denote events lying within the dead zone *undetectable events*, similarly to the case where a given particle has such low energy that it is stopped in the entrance window of the ΔE detector. While these types of events are undetectable in the detector telescope as a whole, the particle still deposits some energy in the ΔE detector. The range of deposited energies E_{dep} corresponding to kinetic energies E_{p} within the dead zone is *not* unique. There exists a range of kinetic energies E_{p} below punch through with the same range of deposited energies E_{dep}, and we shall hence denote this range of deposited energies E_{dep} the *spurious zone* of the detector telescope. Dashed horizontal lines outlining the spurious zone at small and large θ are drawn in the right part of Fig. 1 — from smallest to largest θ, the entire spurious zone spans 600 keV in this example.
- Arrowhead: The particle punches through the ΔE detector, but it *misses* the E detector. As we shall see, the spectra of ΔE-contained events can be severely distorted by this effect. The effect can be avoided if the solid angle coverage of the E detector at least matches that of the ΔE detector, as seen from the particle's point of emission. An event in which a particle deposits some of its energy in the ΔE detector, punches through it and then misses the backing E detector we shall denote a *telescope-missing event*.

Finally, relevant to the characterisation of the dead zone of detector telescopes, we shall from hence forth specifically use the term *punch through* to refer to the scenario in which a particle has sufficient energy to punch through all material layers up to and including the active layer of a ΔE detector (Fig. 1) at a given angle of incidence θ. We shall define the *punch through threshold* as the lowest possible initial particle energy at which punch through can occur for a given θ. Similarly, we shall use the terms *reach through* and *reach through threshold* to refer to the cases where the particle's initial energies are, respectively, sufficient and barely sufficient to reach the active layer of the E detector for a given θ. We shall also, as a useful shorthand, define the term *x μm telescope* to refer to a detector telescope in which the ΔE detector has an active layer thickness of x in units of micrometers. Unless otherwise specified, in all of the following, the employed E detectors have a signal threshold of 100 keV.

3. Distortion from non-backed telescope areas

The final item in the above list, telescope-missing events, comes about when the E detector of a telescope covers a smaller solid angle than the ΔE detector as seen from the point of particle emission. The extents of the detectors and their placement relative to each other and the point of particle emission are ideally such that this scenario cannot occur. In practice, this is not always possible to achieve, and, even if it is, the scenario nicely illustrates some features which are shared with the *inescapable* existence of dead zones between ΔE and E detectors; this latter issue will be covered in Section 4.

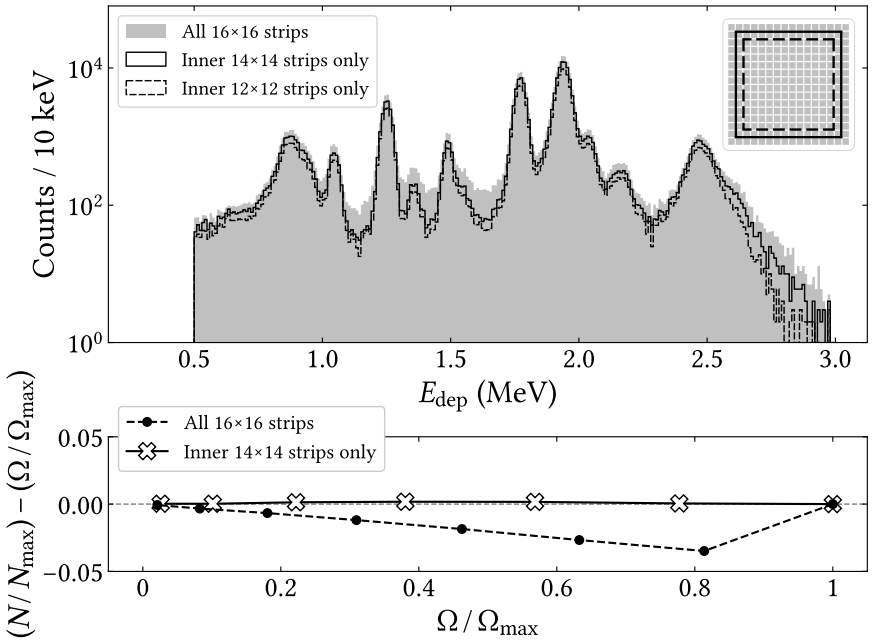

Fig. 2. Top: Energy deposition E_{dep} in 67 μm thick ΔE detector in anti-coincidence with its backing E detector (*ΔE-contained events*). The upper right inset illustrates which strips of the ΔE detector are utilised to produce the spectra. When all 16 × 16 strips are utilised, especially the 1.1 to 1.7 MeV region is heavily distorted. The data are from a decay experiment on ^{21}Mg [9] and are mainly produced by protons emitted from excited states in ^{21}Na. **Bottom:** Deviation from linear relation between number of observed ΔE-contained events N and solid angle coverage Ω, each respectively normalised to the maximum number of observed ΔE-contained events N_{max} and the maximum solid angle coverage Ω_{max}. For the points starting at $\Omega/\Omega_{\mathrm{max}} = 1$ and moving towards 0, the current outermost strips are progressively excluded; as in the top part of the figure.

3.1. Example of the problem

The *non-backed areas* of a given ΔE detector can significantly distort the intermediate energy region of the observed particle spectra. More specifically, the ΔE-contained spectra below the punch through threshold can have regions of significant smearing, obscuring the nuclear structure information otherwise contained there. This is illustrated in the spectra of Fig. 2: The spectra consist of events from different subsets of ΔE strips in which the events are anti-coincident with the corresponding E detector. Based on the definitions of the previous section, we here expect to see ΔE-contained events and, possibly, telescope-missing events. It is crucial to be able to separate telescope-missing events from all other types of events. In the areas of the telescope where the ΔE detector is properly backed by the E detector, telescope events can be identified and, logically, telescope-missing events are not a concern, but in the non-backed areas of the ΔE detector, there is generally no way to distinguish telescope-missing events from ΔE-contained events. The conclusion is that the non-backed areas of the detector telescope must be excluded from the analysis of the particle spectra, reducing the solid angle coverage of the telescope from the otherwise larger solid angle coverage of the ΔE detector to that of the E detector. The recourse, as illustrated in Fig. 2, is more well-defined peaks in the intermediate energy region of the particle spectrum where the telescope-missing events were otherwise responsible for a heavy distortion of the spectrum. The extent and severity of distortion is entirely determined by the relative intensity of particle energies above punch through.

3.2. Validation of ΔE-backing

A simple test to identify the non-backed areas of a detector telescope can be made from the following considerations. For an isotropically emitting source, one expects a linear relation between a certain solid angle and the number of events observed in the solid angle in question; twice the events for a doubling of the solid angle, etc. The true events observable by a detector telescope can be split into the two types of events which we have already defined – ΔE-contained events and telescope events – and these subtypes of events should each obey the same principle. But if one includes the non-backed area of the telescope, the telescope-missing events will add to the true ΔE-contained events. The registered number of ΔE-contained events will thus be erroneously larger in the non-backed areas of the telescope. This is illustrated in the bottom part of Fig. 2 where the normalised deviation from a linear relation between the number of observed ΔE-contained events N and the solid angle coverage Ω is plotted against the normalised solid angle coverage. By only including the innermost 14 × 14 strips, the maximum deviation is roughly 1 per mille instead of 4 percent.

The sort of treatment just outlined can be extended to situations where a symmetric exclusion of detector strips is too simple. By systematically including and excluding certain strips or pixels of a given ΔE detector, the non-backed areas of a given telescope can be accurately mapped. In principle, this allows for the determination of the telescope's position relative to the point of particle emission and offers insight on the spread of the emission point as well. Especially if several detector telescopes are utilised in an experiment, this method offers some constraints on the point of particle emission. If the positioning of the E detector relative to the ΔE detector is uncertain within some bounds, the same method can be used to elucidate that issue.

4. Identifying dead and spurious zones of telescopes

We continue by discussing the issues related to stopping in the dead layers between a detector telescopes' two active layers — the undetectable and spurious events defined in Section 2.3. In that section it was pointed out how the dead and spurious zones of a telescope vary

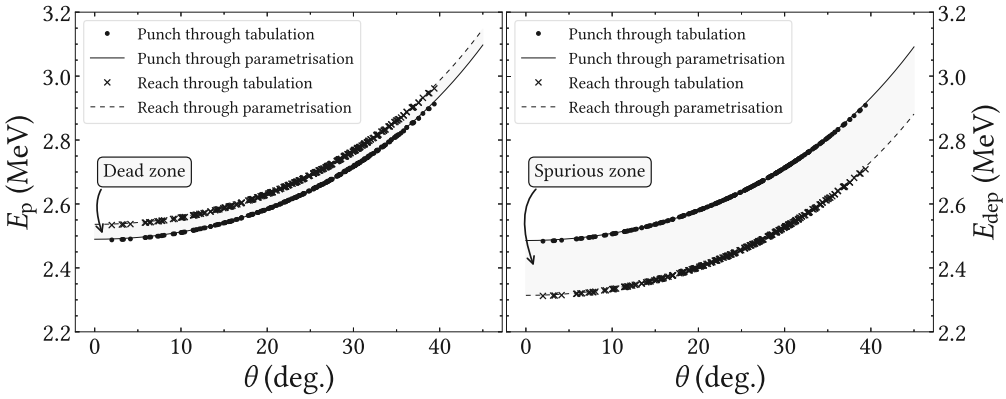

Fig. 3. Left: Example of proton kinetic energies E_p against angle of incidence θ between the point of particle emission and detector surface. These specific proton energies outline the *dead zone* for a telescope with a ΔE detector thickness of 67 μm and a signal threshold of 100 keV on the E detector. Protons with E_p within the dead zone are undetectable (as defined in Section 2.3). **Right:** Corresponding deposited proton energies E_{dep} in the ΔE detector against θ. At and above punch through, E_{dep} will decrease towards the reach through threshold and beyond. For E_{dep} between the punch through and reach through thresholds, the corresponding kinetic energy E_p cannot be uniquely assigned (see Fig. 1). This region of events is hence a *spurious zone* of events. Energy loss tabulations [4] have been utilised to calculate the relevant proton energies for all 256 pixels of the detector and have then been fitted to Eq. (3).

with angle of incidence θ between detector surface and a particle's point of emission. In other words, a θ-dependent gap in the dynamic range of a given detector telescope emerges.

4.1. Parametrisation of dead and spurious zones

Fig. 3 shows an example of the dead and spurious zones for protons outlined by the punch through and reach through thresholds of a telescope consisting of a 67 μm ΔE detector with an effective total dead layer thickness between ΔE and E detector consisting of 0.4 μm silicon, 0.8 μm aluminium and a signal threshold of 100 keV. Energy loss tabulations from SRIM [4] have been utilised to tabulate the punch through and reach through thresholds of the centre of each individual pixel of the ΔE detector. With guidance from the approximation in Eq. (2), a parametrisation of the two angle-dependent thresholds have then been carried out by fitting the tabulations to the expression

$$E(\theta) = E_0 \left(1 + a\frac{1-\cos\theta}{\cos\theta}\right) \tag{3}$$

with $E_0 = S_0 L_0$ the approximate energy loss at $\theta = 0$ and a being a factor which mostly corrects for the otherwise poor approximation in Eq. (2).

A closer visual inspection of Fig. 3 reveals that the parametrisation is not perfect; the residuals between tabulation and parametrisation are as large as 10 keV at the extremes of θ. This deviation can be reduced by adding more terms to Eq. (3). In the end, the simpler form of Eq. (3) was settled upon as deviations of 10 keV near the edges of the dynamic ranges of the individual ΔE and E detectors are insignificant compared to the extents of the dead and spurious zones, the detectors' resolutions, etc. The simple form of Eq. (3) is convenient, as it ensures fast convergence for fits with initial guesses $a = 1$ and $E_0 = \min(\mathbf{E})$, where $\mathbf{E}$ are the dependent variables of the data to be fitted.

4.2. ΔE Thickness estimation from punch through

Fig. 4 shows data for energy depositions E_{dep} against angles of incidence θ in the same 67 μm telescope[1] as in Fig. 3. The data are conditioned on the presence of a signal in the E detector. The maximally possible energy depositions in the ΔE detector for various possible active layer thicknesses have been calculated and then fitted and drawn in Fig. 4 with the same method as in Fig. 3. Comparing these maximally possible energy deposition curves with real data can help to determine the thickness of a detector, as there should be no true events above these curves for the correct detector thickness. Conversely, by drawing these energy deposition curves and confirming the thickness specifications of the ΔE detector, as they may have been given by the manufacturer, one is reassured in the correctness of the range of the dead zone of the telescope in question.

In comparing Figs. 3 and 4, it is important to distinguish the initial particle energy E_p and the deposited energy E_{dep}: Due to the dead layers preceding the active layer of the detector, $E_p(\theta)$ will generally be larger than $E_{dep}(\theta)$. Consider, for instance, the lowest-lying punch through events in Fig. 4, identified by their dependence on θ. These events are due to the largest initial particle energies E_p of the data. Peaks in the E_{dep} spectrum which are independent of θ, on the other hand, stem from particles which deposit all of their energy in the ΔE detector — these are the ΔE-contained events discussed at length in Section 3.

The peak near 2.5 MeV in Fig. 2 is only seen above $\theta \sim 10°$ in Fig. 4 where the effective thickness of the ΔE detector allows for the appearance of the peak in the spectrum. Checking whether peaks appear and disappear above and below the expected angles of incidence like this can, again, serve as a consistency check. This is, however, entirely dependent on the particle spectrum being sufficiently intense around the punch through threshold. It should be noted that the telescope-missing events of Fig. 2 are also present in Fig. 4 at large θ. All punch through events can be removed from the E_{dep} vs. θ spectrum via an anti-coincidence gate with the E detector, as was done in order to produce Fig. 2.

On the subject of thickness estimation of a given ΔE detector, if one draws the same kinds of tabulations as in the right part of Fig. 1 on top of a $\Delta E - E$ spectrum for various assumed thicknesses of the ΔE detector, yet another method of checking the detector thickness presents itself. This is illustrated in Fig. 5 for the same 67 μm ΔE telescope. If the detector geometry is close, and hence the possible angles of incidence θ between detector surface and point of particle emission are large, one can constrain the data on various subintervals of θ and verify the correct displacements and varying curvatures of the curves describing telescope events. Similarly, one can verify the larger possible energy depositions in the ΔE detector for larger θ. In Fig. 5, the telescope event curves are drawn at the lower and upper extremes of angles of incidence θ for the selected data, and since the placement of the curve for $2° \leq \theta \leq 5°$ does not vary much, while the placement of the curve for $33° \leq \theta \leq 39°$ does (Fig. 3), the placement of the curves are as expected within the detector resolutions, etc. The two thin horizontal lines drawn in Fig. 5, where the telescope event curves and ΔE-contained event regions meet, highlight regions

[1] *x μm telescope* defined at the end of Section 2.3.

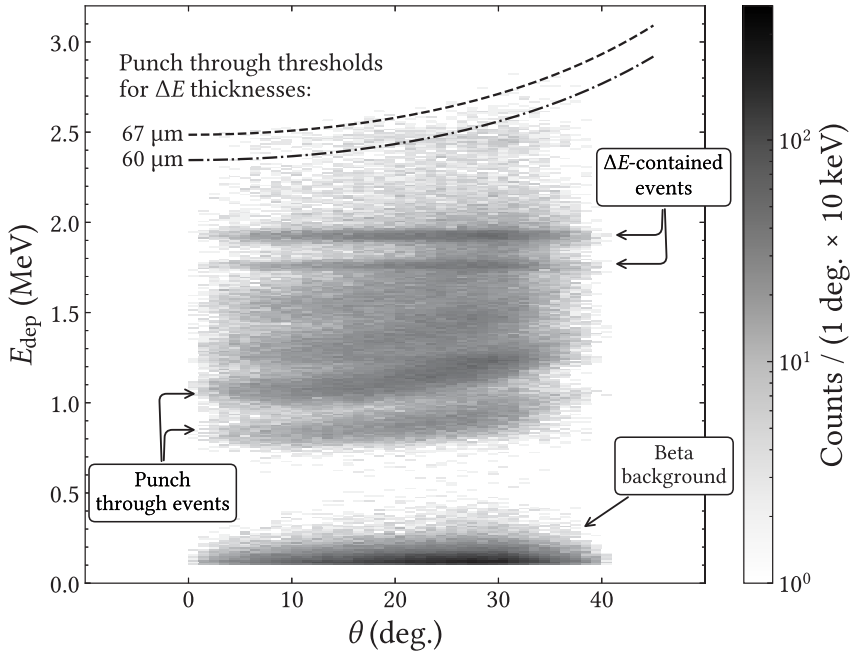

Fig. 4. Energy deposition E_{dep} against angle of incidence θ between the point of particle emission and detector surface in ΔE detector with a thickness of 67 μm. Energy loss tabulations [4] have been utilised to draw the punch through threshold curves using the same fitting procedure as exemplified in Fig. 3. The data are from the same experiment as referenced in Fig. 2 where beta particles and protons are primarily observed in the detector telescopes. In order to be able to illustrate the presence of punch through events, events in anti-coincidence with the E detector (pure *ΔE-contained* events) are not shown here. The ΔE-contained events hence stem from random coincidences with the E detector or from true coincidences where the beta particles are detected in the E detector.

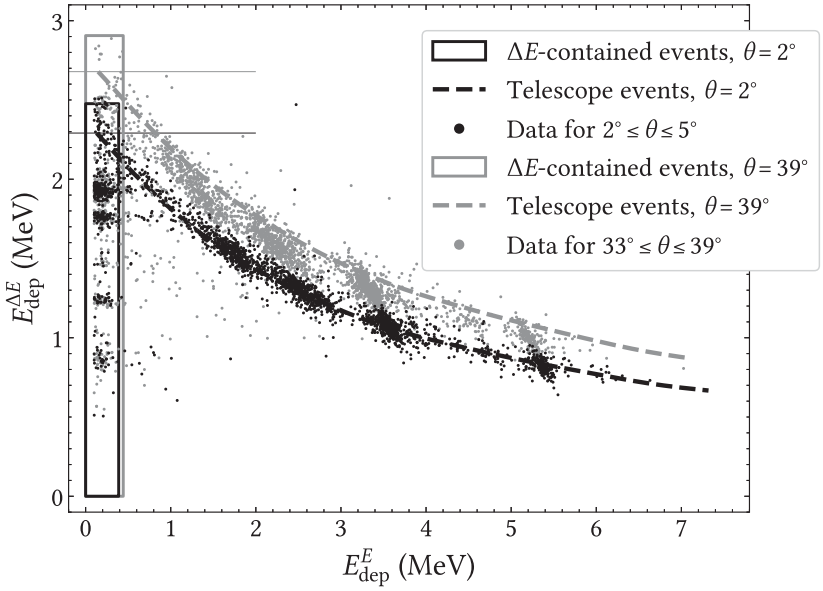

Fig. 5. Energy deposition in ΔE detector $E^{\Delta E}_{dep}$ against energy deposition in E detector E^{E}_{dep} for detector telescope at different angles of incidence θ between the point of particle emission and detector surface. The ΔE detector has a thickness of 67 μm and the E detector has a signal threshold of 100 keV. The boxes outlining the ΔE-contained events and the curves defining the telescope events have been drawn solely based on energy loss tabulations from SRIM [4] and knowledge of the dead layer thicknesses and signal thresholds, assuming an active layer thickness of 67 μm in the ΔE detector. The data are from the same experiment as referenced in Fig. 2 where protons can be identified by the $\Delta E - E$ technique. The constraints on θ are chosen such that there are roughly the same number of events (around 3000) in both intervals.

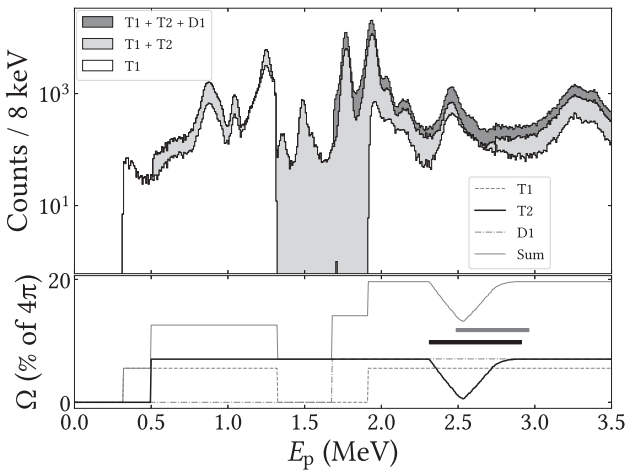

Fig. 6. Top: Beta-delayed proton energy spectrum of ^{21}Mg at low to intermediate proton kinetic energies E_p as observed by two detector telescopes and one thick DSSSD. The data are from the same experiment as referenced in Fig. 2 where protons emitted from excited states in ^{21}Na are primarily observed. In the figure legends, *T1* is short for *42 μm telescope*, *T2* is short for *67 μm telescope*, and *D1* is short for *1000 μm DSSSD*. **Bottom:** The corresponding energy-dependent solid angle coverage Ω of the detector telescopes and the thick DSSSD. The extents of the spurious zone (black) and the dead zone (grey) are indicated for the 67 μm telescope with the thick lines lying between 2.3 and 3.0 MeV. Taken as a whole, the top and bottom panels illustrate the results of properly accounting for all challenges, as described in this paper, associated with extending the energy spectra of detector telescopes below their punch through thresholds. The variations in solid angle coverage with energy can, if they are not taken into consideration, give a misrepresentation of the underlying nuclear structure. See text for a more detailed discussion.

of energy deposition in the ΔE detector that can never coincide with a true signal in the backing E detector — this is merely yet another way of visualising the spurious zone between the two detectors as in Figs. 1 and 3.

5. Combining telescope spectra

After telescope- and ΔE-contained events have been properly separated and when dead zones and spurious zones of the detector telescopes have been identified, the groundwork has been laid for combining the observed energy spectra into one complete spectrum, where above- and below-punch through events can be treated on an equal footing. By mapping the energy-dependent solid angle coverage of each detector configuration,[2] one can combine the energy spectra of the detector configurations into an all-encompassing spectrum like the one shown in Fig. 6. The figure shows the combined beta-delayed proton energy spectrum of ^{21}Mg as observed by two detector telescopes and one thick DSSSD all situated near the point of particle emission. The solid angle coverage Ω of the entire setup varies with the kinetic energies E_p of the protons. The total spectrum ranges up to roughly 9 MeV, but here we wish to highlight the varying solid angle coverage at low to intermediate energies.

In Fig. 6, the solid angle coverage for all detector configurations are initially zero, as an energy cutoff has been set in order to separate betas from protons (Fig. 4). The detectors then become active above their energy cutoffs. The cutoff for the thick DSSSD is larger than what would be necessitated by minimum ionising beta particles alone; it is due to the positioning of the detector directly below the target frame on which particles scattered during the experiment. The reduction in solid angle coverage of the thick DSSSD due to the shadow generated by the target frame is taken into account.

[2] Detector configuration in this case refers either to a detector telescope or to a DSSSD which is not backed by any detector.

In Fig. 6, the varying solid angle coverage for the 67 μm telescope is nicely illustrated for particle energies spanning the dead and spurious zones depicted in Fig. 3, ranging from $E_p \sim 2.3$ MeV up to $E_p \sim 3.0$ MeV. Note that although the solid angle coverage does approach zero in this region, at least a small fraction of the detector telescope is active throughout. Having properly characterised this 67 μm telescope, the proton energies lying in the telescope's dead and spurious zones do not have to be neglected entirely. Rather, the proton energies which remain detectable at certain angles of incidence θ (Fig. 3) also remain part of the combined energy spectra, but only under consideration of the energy-dependent solid angle coverage additionally present in this region. Note also in Fig. 6 that the dead and spurious zones of the 67 μm telescope broadly overlap. This is the case for the telescope as a whole, but for an individual pixel of the ΔE detector, the dead and spurious zones are disjoint sets with the upper end of the spurious zone barely touching the lower end of the dead zone — see Fig. 3. The two zones are complementary, but the spurious zone spans a larger range due to the inability to uniquely assign a particle energy E_p to any given deposited energy E_{dep} between punch through and reach through, as is evident from Fig. 1.

The solid angle coverage of the 42 μm[3] telescope in Fig. 6 should have seen a similar kind of variation with energy, but it was decided to entirely exclude deposited energies in the ΔE detector above 1.3 MeV — hence the drop of solid angle coverage to zero. The reason for excluding the energy region is a seemingly non-uniform thickness across the detector surface. Identification of punch through events seem indicative of an active layer thickness as small as 30–35 μm in the centre of the detector, but approaching the 42 μm, stated by the manufacturer, near the edges of the detector. The limit of 1.3 MeV has been set based on the extremes of the dead and spurious zones tabulated for a 30 μm telescope. Whether the apparent variation in thickness of the ΔE detector is in fact due to a ∼20% variation of the detector thickness, or if it is perhaps due to incomplete depletion of the active medium is not known, as the detector has not been readily available when the present analyses were carried out. While the solid angle coverage of the 42 μm telescope is not exactly illustrative of the methods developed in this paper, the method of combining energy spectra of several detector telescopes should still be clear from the ideal example presented via the 67 μm telescope and from the prerequisite methods outlined earlier in this paper. For the purposes of the nuclear physics results published separately [9], all events are internally consistent within the 42 μm telescope when the spurious energy region is excluded, and the resulting energy spectra are consistent with those of the other detector configurations as well.

Finally we note, with reference to Fig. 6, that when all detectors are active and when the punch through thresholds of all detector telescopes have been overcome, the solid angle coverage remains constant. In principle, the solid angle coverage will taper off as the particles begin to punch through the E detectors of the telescope, but this is irrelevant under most practical circumstances.

6. Summary and outlook

The problems involved in extending the energy spectra of silicon strip detector telescopes below punch through of the involved ΔE detectors have been investigated and methods to overcome these problems have been presented. This was done in the context of beta-delayed proton emission from ^{21}Mg, which has a wide distribution of energy levels across the entire dynamic range both of the $\Delta E - E$ telescope and of the ΔE detector by itself. It was argued that the two parameters which, more than anything else, characterise the data extracted from modern detector telescopes employed in close geometry are (1) the active layer thicknesses of the ΔE detectors, and (2) the signal thresholds of the E detectors. The potential distortion of the below-punch through

[3] Stated thickness.

energy spectrum of detector telescopes from telescope-missing events was illustrated, and it was shown how, in such a case, the non-backed areas of a given ΔE detector can be mapped by systematically including and excluding events from its strips and comparing the number of ΔE-contained events to the resulting varying solid angle coverage.

The closer the detector geometry of a given setup, the greater the range of angles of incidence θ between point of particle emission and detector surfaces. The θ-dependent active layer thickness of a given ΔE detector in combination with the signal threshold of its backing E detector can, for sufficiently close detector geometries, result in the appearance of dead and spurious zones spanning several hundreds of keV. Within the dead zone of a detector telescope, certain particle energies E_p are undetectable. The spurious zone, an accompaniment to the dead zone, defines a range of deposited energies E_{dep} in a given ΔE detector in which the corresponding particle energies E_p cannot be uniquely assigned. For a given detector telescope as a whole, the spurious zone generally spans a broader range of particle energies E_p than does the dead zone.

It was shown how the θ-dependent dead and spurious zones can be parametrised, and the parametrisation procedure was extended to allow for the determination of the active layer thicknesses of ΔE detectors through comparison with observed data. The separation of true ΔE-contained events and true telescope events as well as the identification of θ-dependent undetectable and spurious events in telescope dead and spurious zones ensures the integrity of data extracted from detector telescopes. As a result of this, it was shown how the particle energy spectra of several detector telescopes can be combined into one complete particle energy spectrum where the energy-dependent variation in solid angle coverage must be – and can be, due to the developed methods – taken into consideration. For the example of beta-delayed proton emission from ^{21}Mg the entire particle energy spectrum from the proton separation threshold of ^{21}Na to the Q-value of the decay can be investigated only by extending the telescope spectra below their punch through thresholds.

6.1. List of recommendations

In summary, we recommend the following steps when setting out to extend the particle spectra of $\Delta E - E$ detector telescopes below their punch through thresholds:

1. Map the non-backed areas of the ΔE detectors of each telescope, thus potentially filtering out telescope-missing events from the ΔE-contained events.
2. Estimate the thicknesses of the employed ΔE detectors by:
   (a) Tabulating maximally possible energy depositions for various active layer thicknesses of the ΔE detectors and comparing with real data.
   (b) Tabulating the expected energy depositions in the E detectors for various active layer thicknesses of the ΔE detectors and comparing with real data.
3. Tabulate the dead zones and spurious zones of each detector telescope.
4. Reject events lying within these zones and estimate the resulting energy-dependent reduction in solid angle coverage.

By following these steps, one is assured in the correctness of the particle energy spectra extracted below punch through threshold, and further analyses of the data in question can be carried out.

6.2. Thickness non-uniformity of thin silicon strip detectors

As was mentioned towards the end of Section 5, there were indications of a non-uniform active layer thickness of one of the employed ΔE detectors. Thickness non-uniformity of thin silicon strip detectors has recently been investigated e.g. in Ref. [15]. The methods developed in the present paper generally assume a uniform active layer thickness where the effective variation in thickness stems from the variation in angle of incidence θ between point of particle emission and detector surface. The methods can, however, in principle be extended to map the active layer thickness of the individual pixels of a given ΔE detector, given a sufficiently large data set per pixel. The methods' dependence on the distribution of particle energies following the decay of a given radioisotope could be avoided entirely, for example, by devising investigative experiments similar to the ones in Ref. [15]. There, the authors scatter 40 and 55 MeV ^{12}C on a gold foil, which, from a simple elastic scattering calculation, yields scattered particle energies in the range 32–40 (44–55) MeV for scattering angles between 0 and 180 degrees for projectile energies of 40 (55) MeV. For a lighter projectile, such as a proton, on gold, the variation in scattered particle energies can be brought to the order of typical silicon detector energy resolutions. In principle any combination of projectile, projectile energy and target can be utilised, provided that the punch through threshold can be exceeded. By varying the projectile energy around the relevant punch through thresholds of detector telescopes, the pixels at varying angles of incidence will be characteristically active or inactive given the active layer thickness of each pixel, and hence the individual pixel thicknesses can be mapped.

As a final remark we note that while the methods presented in this paper allow the entire dynamic ranges of detector telescopes, including the telescope dead and spurious zones, to be utilised, setups in which several detector telescopes are employed might still benefit from containing ΔE detectors of active layer thicknesses which differ to such an extent that the dead and spurious zones of the individual telescopes do not overlap. In that case, an additional assurance of data integrity of a detector telescope can be attained by comparison with another telescope where the relevant particle energies are not within each others' dead and spurious zones.

Declaration of competing interest

The authors declare that they have no known competing financial interests or personal relationships that could have appeared to influence the work reported in this paper.

Data availability

Data will be made available on request.

Acknowledgements

We acknowledge funding from the Independent Research Fund Denmark (9040-00076B and 2032-00066B). We thank our colleagues from the ISOLDE IS507 experiment from where the ^{21}Mg data originated.

References

[1] F.S. Goulding, D.A. Landis, Ann. Rev. Nucl. Sci. 25 (1975) 167.
[2] D.G. Perry, L.P. Remsberg, Nucl. Instrum. Methods 135 (1976) 103.
[3] A. Badalà, et al., Riv. Nuovo Cimento 45 (2022) 189.
[4] J.F. Ziegler, et al., Nucl. Instrum. Methods Phys. Res. B 268 (2010) 1818.
[5] Stopping powers and ranges for protons and alpha particles, ICRU report 49, J. ICRU (1993).
[6] Stopping of ions heavier than helium, ICRU Report 73, J. ICRU (2005).
[7] B. Blank, M.J.G. Borge, Prog. Part. Nucl. Phys. 60 (2008) 403.
[8] M. Pfützner, et al., Rev. Modern Phys. 84 (2012) 567.
[9] E.A.M. Jensen, et al., The beta decay of ^{21}Mg, 2023, Manuscript, (in preparation).
[10] M.V. Lund, et al., Eur. Phys. J. A 51 (2015) 113.
[11] O. Tengblad, et al., Nucl. Instrum. Methods Phys. Res. A 525 (2004) 458.
[12] M.V. Lund, et al., Eur. Phys. J. A 52 (2016) 304.
[13] S. Viñals, et al., Eur. Phys. J. A 57 (2021) 49.
[14] U.C. Bergmann, et al., Nucl. Instrum. Methods Phys. Res. A 515 (2003) 657.
[15] Q. Liu, et al., Nucl. Instrum. Methods Phys. Res. A 897 (2018) 100.